Biosensors and Bioelectronics 280 (2025) 117460



Contents lists available at ScienceDirect

Biosensors and Bioelectronics

journal homepage: www.elsevier.com/locate/bios



"Sample-in, result-out" liquid biopsy chip based on immunomagnetic separation and CRISPR detection for multiplex analysis of exosomal microRNAs

Niancai Peng [a,c], Xueqin Gao [b], Zhang Yong [b], Yunyun Zhang [c], Xiaoniu Guo [a], Qiaochu Wang [a], Yong Wan [d], Shuhao Zhao [a], Tianyi Zhang [a], Fei Hu [a,*]

[a] State Key Laboratory for Manufacturing Systems Engineering, School of Instrument Science and Technology, Xi'an Jiaotong University, Xi'an, 710054, Shaanxi, China
[b] State Key Laboratory for Manufacturing Systems Engineering, School of Mechanical Engineering, Xi'an Jiaotong University, Xi'an, 710054, Shaanxi, China
[c] Xi'an Key Laboratory of Biomedical Testing and High-End Equipment, Xi'an, 710049, Shaanxi, China
[d] Department of Geriatric Surgery, First Affiliated Hospital, Xi'an Jiaotong University, Xi'an, 710054, Shaanxi, China

ARTICLE INFO

Keywords:
Exosome isolation and detection
IISA
CRISPR/Cas13a
Multiplex miRNA analysis
On-chip liquid biopsy

ABSTRACT

Multiplex analysis of exosomal microRNAs (miRNAs) plays an important role in noninvasive early disease diagnosis. However, the complexity of the testing process has hindered its clinical application. Here, we proposed an integrated chip for the detection of eight exosomal miRNAs in serum which can achieve "sample in, result out" detection. We developed an immunomagnetic isolation system based on CD63 aptamers (IISA) for separation of serum exosomes. The system was combined with immiscible filtration assisted by surface tension (IFAST) to remove impurities. Bubble mixing was applied to ensure adequate binding or cleavage of exosomes to magnetic beads. CRISPR detection technology was utilized to allow for effective detection of seven hepatocellular carcinoma (HCC)-related miRNA targets. Based on the test of clinical samples, the chip can achieve 78 % exosome capture efficiency and 55 % recovery, and simultaneously detect eight targets within 1 h. This chip could be applied as a robust and cost-effective tool for cancer diagnosis and monitoring of cancer stages.

1. Introduction

Exosomes are nano-sized, lipid-bilayered vesicles secreted by cells with diameters typically ranging from 30 to 150 nm (Yu et al., 2021a). Exosomes originate in cells and are discharged into bodily fluids following membrane fusion; they are ubiquitously present in various fluids such as blood, urine, and saliva (Jablonska et al., 2019). Recent research has highlighted the pivotal role of exosomes and their cargos in diagnosing and treating cancer and other related diseases (Keerthikumar et al., 2016). The levels of specific exosome types, the expression of microproteins, and the profile of miRNAs have been reported to correlate with the progression of multiple cancers, including liver, breast, and prostate malignancies (Kalluri and LeBleu, 2020). In recent years, exosomes have been used as important biomarkers in non-invasive liquid biopsy for early detection of hepatocellular carcinoma (HCC) (Sasaki et al., 2019). The number of exosomes varies with tumor progression, and their molecular content also plays a key role in tumor evolution. This aids in the understanding of mechanisms of HCC and the identification of targets for therapeutic interventions. Unlike free nucleic acid molecules, the lipid bilayer of exosomes functions to protect the internal contents, keeping proteins and nucleic acids to remain active and undegraded (Weber et al., 2010).

Nucleic acids in exosomes, particularly RNAs, are crucial for cellular communication and detection (O'Brien et al., 2020). Among various types of RNAs, miRNAs (<200 bp) are non-coding RNAs that regulate gene expression by binding to the 3′ untranslated regions (UTRs) of the target mRNAs and controlling various metabolic and disease processes. For example, miR-21 and miR-192 regulate the developmental process of HCC by acting on target genes (Lee and Brianna, 2024; Liu et al., 2020). The upregulation of miR-26 and downregulation of miR-223 promote angiogenesis and thus HCC (Fu et al., 2023; Yang et al., 2014). And miR-27, miR-122, and miR-155 are involved in cancer development by regulating cell proliferation and tissue migration. These miRNAs have different expression levels as the cancer progresses (Bhattacharya et al., 2016; Öksüz et al., 2023; Wang et al., 2016; Xu et al. 2011, 2018; Zhang et al., 2019a) and thus can be used as molecular

* Corresponding author.
E-mail address: hufei0701@xjtu.edu.cn (F. Hu).

https://doi.org/10.1016/j.bios.2025.117460
Received 12 February 2025; Received in revised form 7 April 2025; Accepted 7 April 2025
Available online 8 April 2025
0956-5663/© 2025 Elsevier B.V. All rights are reserved, including those for text and data mining, AI training, and similar technologies.

markers to obtain more information about HCC. Intensive mechanistic studies have highlighted the strong correlation between miRNAs and HCC, emphasizing their potential in diagnosis, treatment, and prognosis.

Efficient exosome isolation is vital for research and clinical use. Current methods - including ultracentrifugation, immunoprecipitation, polymer precipitation, and size exclusion chromatography - typically exhibit low yield, poor purity, and complex workflows (Baranyai et al., 2015; Sidhom et al., 2020). Recently, selective adsorption of magnetic beads has been proposed to separate exosomes (Fang et al., 2021). Immunomagnetic separation using antibody-coated magnetic beads provides high-purity exosomes and non-destructive release, but the antibodies are costly and the modification process is laborious (Guo et al., 2023). Aptamer-modified magnetic beads have been developed to overcome these limitations, offering an efficient, cost-effective, and user-friendly exosome capture approach. For example, Zhang et al., (2019b) designed a DNA aptamer-based system that captures and releases exosomes within 90 min, with a separation efficiency of 78 %; nonetheless, the system is time-consuming. Additionally, these methods face challenges in portability and integration with other miRNA assays.

Exosomal miRNAs carry valuable pathological information and serve as crucial markers in cancer diagnosis. However, the miRNA expression levels are influenced by multiple factors and largely varied, it is not possible for diagnostic detection to rely on targeting a single type of miRNA. By combining multiple miRNA targets, diagnostic accuracy can be enhanced, which is vital for precision medicine (Gao et al., 2020). The detection of miRNAs has made great progress in recent years. Among all techniques with integrated nucleic acid amplification, the most prominent techniques include quantitative reverse transcription-polymerase chain reaction (qRT-PCR) (Pritchard et al., 2012), rolled-loop amplification coupled with CRISPR and CRISPR-associated enzymes (RCA-CRISPR/Cas) (Wang et al., 2020), and exponential amplification in conjunction with CRISPR/Cas systems (EXPAR-CRISPR/Cas) (Yang et al., 2022). However, these methods require strict temperature control and specialized equipment, limiting their integration into diagnostic platforms. Their complex workflows also risk contamination and reagent loss during uncapping/transfer steps, potentially affecting assay accuracy (Zhao et al., 2020). Among all the CRISPR/Cas systems, Cas13a stands out as the sole RNA-targeting enzyme (Wu et al., 2021). It has been widely applied across diverse detection domains, encompassing nucleic acids (Yuan et al., 2020; Zhou et al., 2020) and viruses (Qin et al., 2019). Shan et al., (2019) proposed an amplification-free CRISPR/Cas13a method for miRNA detection that achieves reliable and sensitive detection within 30 min with a LOD of 4.5 aM. This method can be easily implemented and holds great potential for the early diagnosis of miRNA-related diseases. However, it has not been applied to the detection of multiple targets.

The advent of microfluidic chip technology heralds a new era for the integration and portability of experimental processes (Kaarj et al., 2018; Ulep et al., 2020). This technology has broad applications in exosome separation and detection. Woo et al., (2017) employed a dual-layer filtration system to enrich 20–600 nm vesicles from blood, achieving >95 % efficiency. However, the chip suffered from clogging, limited sample capacity, and short lifespan. Yu et al., (2021b) introduced an integrated Exosome Separation and Detection (ExoSD) chip by leveraging magnetic bead immunocapture for effective exosome isolation from flowing samples. To streamline on-chip washing and purification, researchers devised the IFAST technique (Berry et al., 2011a) by utilizing a stabilized two-phase interface in microchannels to filter surface contaminants from magnetic beads to replace conventional washing steps. This technology has since been widely utilized in sorting and purifying small molecules, including bacterial (Ngamsom et al., 2017), cellular (Berry et al., 2011b), and viral RNA molecules (Berry et al., 2014). In our previous exosome isolation chip, IFAST technology has been used to filter impurities for purification of exosomes (Guo et al., 2024).

In this study, we developed an integrated chip combining magnetic separation and CRISPR technology for the enrichment and high-purity retrieval of exosomes from human serum and detections of multiple miRNAs (Fig. 1). To maximize on-chip exosome recovery, we proposed an immunomagnetic isolation system based on CD63 aptamers, which integrates IFAST and gas-phase mixing, and achieved a 78 % capture efficiency and a 55 % exosome recovery. The CRISPR/Cas13a system was used for direct detection of seven HCC-associated miRNA targets. By designing eight chambers for spatial multiplexing, rapid simultaneous detection of eight miRNAs can be achieved. The chip was also applied to detect clinical samples. The whole process could be completed on the chip within 1 h, allowing for the rapid sample-to-result detection and diagnosis of HCC patients based on eight miRNAs.

2. Materials and methods

Please see supporting information for the details.

3. Results and discussion

3.1. Working principle of the chip

The integrated chip combines IISA and CRISPR technologies for the rapid separation and detection of exosomes in serum samples from cancer patients. Exosomes are captured by IISA, and impurities are removed by the IFAST technology. The use of mixing assisted by gas phase (MAGP) enhances the binding and improves the separation and lysis efficiency. Liquid transfer through negative pressure (LTNP) facilitates the transfer of the lysate to the detection chambers for CRISPR reactions. This system allows for gentle, rapid isolation and purification of exosomes, and highly sensitive, on-chip detection of eight miRNAs.

Fig. 1 depicts the schematic illustration of the on-chip isolation and detection of exosomes. Samples, silicone oil, buffer solutions, and lyophilized reagents are preloaded into the corresponding chambers. The generation of bubbles accelerates the motion of fluid in the vicinity, enhancing the binding between the aptamers on the bead surface and exosomes. The magnetic force, generated by a permanent magnet, is applied to the beads to overcome the surface tension and fluid resistance, enabling them to traverse the IFAST region. The surface tension at the two-phase boundary prevents hydrophilic (or hydrophobic) impurities from crossing the immiscible interface, thus eliminating nonspecific contaminants with poor adhesion to the surfaces of the magnetic beads. And buffer W can also be used for washing to remove impurities. Upon reaching the recovery chamber, exosomes are lysed sufficiently with the aid of bubble mixing to release miRNA (For exosome analysis without lysis, complementary sequences of CD63 aptamer are used to detach Strep-tag II to release exosomes from magnetic beads). Subsequently, using a negative pressure air pump, the buffer solution containing microRNAs is transferred from the recovery chamber to the detection chambers, where CRISPR/Cas13a-based detection of eight miRNAs takes place at 37 °C using a heating plate. Eight lyophilized crRNA-Cas13a reagents are pre-embedded in separate detection chambers. Only the specific target can bind to the crRNA and activate Cas13a, leading to reporter cleavage and fluorescence production. This approach ensures miRNA-specific reactions and enables the simultaneous detection of eight miRNAs.

The chip is designed in a disk shape to facilitate the repeated transfer of magnetic beads, improving exosome recovery and space utilization. A key feature of the chip is the fan-shaped design of detection chambers, which ensures even distribution of the sample to each chamber, improving the reproducibility and accuracy. Separate detection chambers effectively isolate different reactions, reducing the risk of cross-contamination. Another one lies in mixing structure, where parallel nozzle arrays are arranged at the bottom of the capture/recovery chambers for high-throughput bubble generation. Air injected into the chamber gradually expands due to gas-liquid interfacial tension. The sudden change in structural dimensions at the channel-chamber

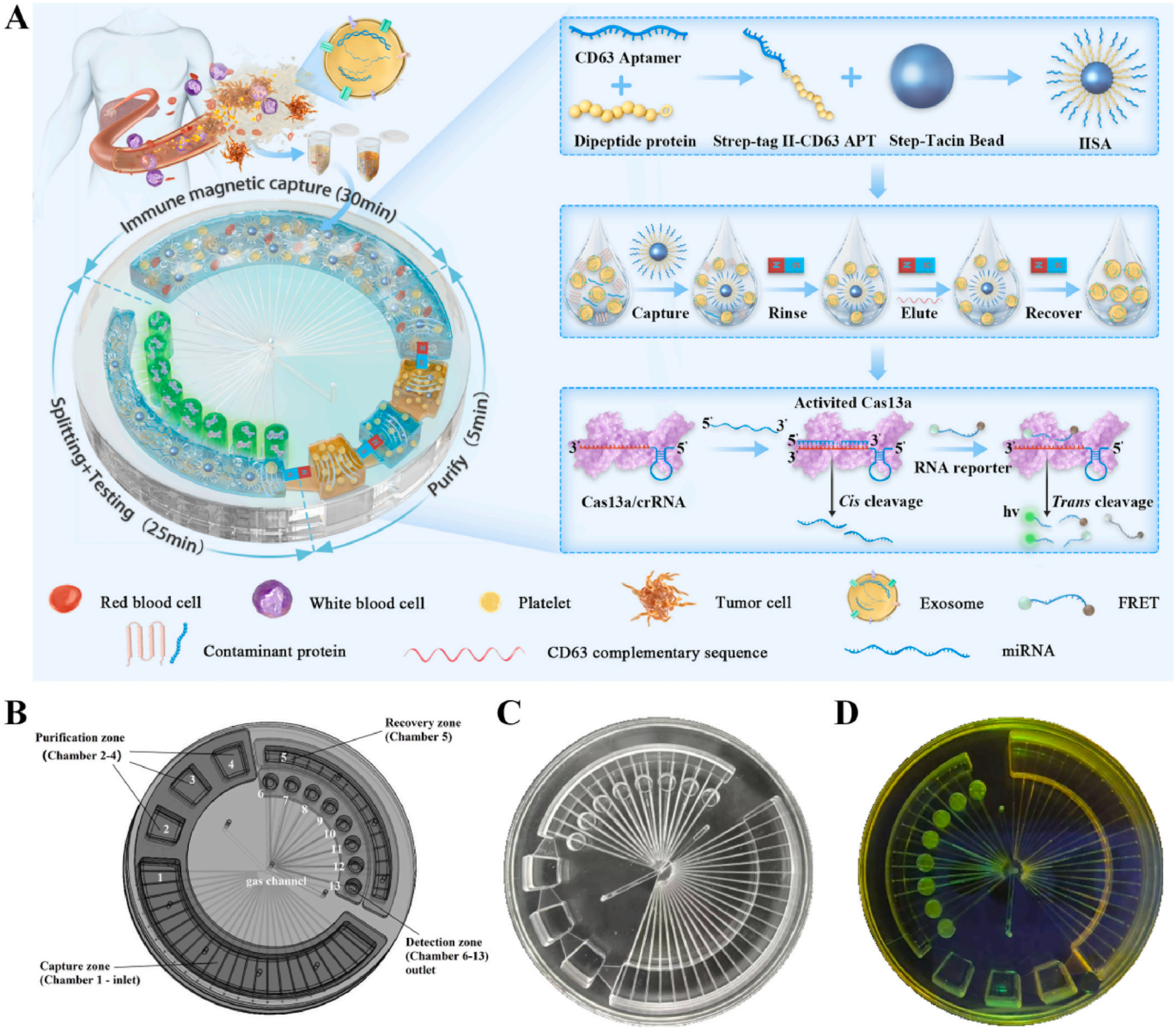


Fig. 1. Schematic diagram of the chip for exosome isolation and detection **from serum.** (A) (1) Exosomes from HCC patient samples are bound to CD63 aptamer-modified magnetic beads in the capture zone with the aid of bubble mixing; (2) Magnetic beads carrying exosomes are filtered through immiscible phase interfaces; (3) Exosomes are lysed in the recovery chamber with the aid of air bubbles mixing; (4) miRNAs from lysed exosomes are drawn into the eight detection chambers for CRISPR reactions under negative pressure. (5) Cas13a/crRNA recognizes the target miRNAs and cleaves the reporters, which exhibits fluorescence. (B) Schematic illustration of the chip configuration. (C) Photograph of the chip. (D) Image of clinical samples tested on the chip.

interface causes an imbalance in gas pressure inside and outside the nozzle. This leads to the gas breaking up and forming monodisperse bubbles due to the Plateau–Rayleigh instability mechanism. The generated bubbles start to increase and rise from the bottom due to buoyancy, perturbing the surrounding fluid and generating micro-vortices, which enhances the effectiveness of the mixing between the beads and exosomes.

3.2. IISA-based exosome isolation and purification

The phospholipid membrane of exosomes is decorated with numerous biomolecules (proteins, lipids, etc.), and this provides an excellent opportunity for highly selective isolation of exosomes (Zhao et al., 2024). We modified the CD63 aptamers onto Strep-Tactin magnetic beads using Strep-tag II short peptides. Strep-Tactin Magnetic Beads have a strong affinity for Strep-tag II, a short peptide tag consisting of only 8 amino acids. The Strep-tag II binds to the 3′ end of the CD63 aptamer through a dehydration condensation reaction, generating the intermediate product Strep-tag II-CD63 aptamer. Subsequently, the -COOH group in the glutamate (Glu) residue of Strep-tag II attaches to the Strep-Tactin protein on the surface of the magnetic beads, resulting in the stable binding of the CD63 aptamer to the bead surface. The affinity between the CD63 aptamer and exosomes is 17.1 nmol/L (Zhang et al., 2022), this modification allows the aptamers on the beads to selectively capture exosomes expressing CD63 on their surface while minimizing nonspecific binding of other sample components. CD63 aptamer-based exosome isolation methods have been validated for specificity and are widely used in recent studies (Cao et al., 2025; Qian et al., 2023; Yu et al., 2024). These established a performance benchmark for evaluating our methodology.

To demonstrate the changes in the magnetic beads before and after Strep-tag II and CD63 aptamers modification, we characterized the

beads using transmission electron microscopy (TEM). As shown in Fig. 2A, unmodified magnetic beads had a regular spherical shape with uneven bumps and pits, possibly due to streptavidin impurities or nonspecific adsorption. In contrast, the modified bead had a smoother surface. The TEM characterization of magnetic beads, post-exosome capture by IISA, revealed vesicle-like protrusions on their surfaces, as shown in Fig. 2B. These features matched exosome size and shape (Characterization of standard exosomes is shown in Fig. 2C), contrast with pre-capture TEM images. Following multiple elutions with CD63 aptamer complementary sequence solution, TEM was employed to inspect the morphology of the released exosomes. According to Fig. 2D, the exosomes had an elliptical shape with a diameter of about 100 nm, which matches the standard exosome samples. This demonstrates the validity of the elution method. The effectiveness of the method can also be demonstrated through the characterization of magnetic beads after capture and elution (Fig. S3). Western blot analysis was employed to target the proteins CD63 and TSG101 after elution, with standard exosomes served as the positive control (PC). Intense bands (Fig. 2E) indicated high expression levels of these proteins, suggesting the substantiating presence and enrichment of exosomes after elution. To assess their biological functions, cellular uptake assays were performed on exosomes and images (Fig. S4) confirms that exosomes retained structural integrity and biological activity after purification and elution. To assess the exosome capture and recovery efficiency of IISA, we used Nanoparticle Tracking Analysis (NTA) to measure the size and concentration of exosomes after capture and elution. Fig. 2F shows the size and concentration distribution of exosomes after capture and elution, with standard exosomes as a control, indicating a capture efficiency of about 55 % and a recovery rate of 43 %.

To maximize the exosome isolation efficiency, parameters including aptamer concentration, magnetic bead amount, aptamer modification time, and exosome capture time were optimized using the control variate method. The time for IISA preparation (F1) and exosome capture (F2) was set at 1 h firstly and the concentrations of the magnetic beads used were all 1 × . Fig. 2G demonstrates the exosome capture efficiency of IISA prepared with CD63 aptamer concentration at 0.1–100 nM. The capture efficiency increased with the increase of aptamer concentration and reached peak value at 10 nM aptamers with an efficiency of ~75 %. Excessively high CD63 aptamer concentrations were found to result in a lower capture efficiency, possibly due to the overly dense modifications which can affect the specific binding of exosomes. The amount of magnetic beads (1 ×) in the capture system was varied from 100 μL to 300 μL with five gradients, and the magnetic beads of each group were resuspended to 198 μL with PBS after magnetic separation. Fig. 2H shows that the capture efficiency reached peak value of about 77 % when the amount of magnetic beads was 200 μL and decreased significantly with the further increase of the amount of magnetic beads. The capture performance is also affected by IISA preparation time affect. As shown in Fig. 2I, the capture efficiency reached peak of about 78 % when F1 was increased to 30 min, but decreased significantly when F1 was further increased. Prolonged modification may cause excessive steric hindrance, impairing exosome-aptamer binding. As illustrated in Fig. 2J, the capture efficiency reached the maximum value at about 75 % with a 30-min incubation (F2), declining with longer durations due to CD63 aptamers performance degradation on the magnetic beads. To improve the elution efficiency, we optimized two key parameters in the exosome elution process, including elution time and eluent concentration. The elution time was optimized initially, and Fig. 2K shows the exosome elution efficiency at different times from 10 to 50 min. The elution efficiency reached ~65 % at the elution time of 20 min, with no further significantly increase for longer elution times. Although the elution efficiency is slightly improved when the elution time reaches 50 min, 30 min was chosen as the optimal elution time to balance efficiency and time cost. Next, we optimized the eluent concentration by measuring the elution efficiency of different CD63 aptamer complementary sequence solutions from 0.1 nM to 1000 nM. We found that the elution efficiency peaked at ~73 % when the concentration was 10 nM (Fig. 2L), which highlights the importance of precise concentration regulation in order to maximize exosome production. Optimizing parameters in the exosome capture and elution process yields an optimal capture efficiency of ~78 % and a recovery rate of ~57 %.

3.3. CRISPR/Cas13a-based microRNA detection

Cas13a enzymes, part of the Class II CRISPR/Cas system, can be assembled with crRNA to form crRNA-guided, RNA-activated HEPN-independent nucleases. The crRNA can be specifically recognized by the target RNA. This recognition activates Cas13a, leading to the non-specific cleavage of the FQ-5U reporter in the system, which separates the fluorescent and quenching groups and exhibits the fluorescent signals. Seven miRNA targets associated with HCC were selected for research, including miR-21, miR-192, miR-26a-1, miR-27a, miR-155, miR-122, and miR-223. MiR-16 was used as an internal reference. And the roles of these miRNAs are summarized in Table S5. To demonstrate that the eight miRNAs do not interfere with each other during reactions, we conducted crossover experiments. Fig. 3A-H depict the fluorescence curves of eight miRNAs obtained by real-time fluorescence monitoring. The fluorescence was generated only when the crRNAs paired with their corresponding miRNAs, demonstrating the specificity of the detection.

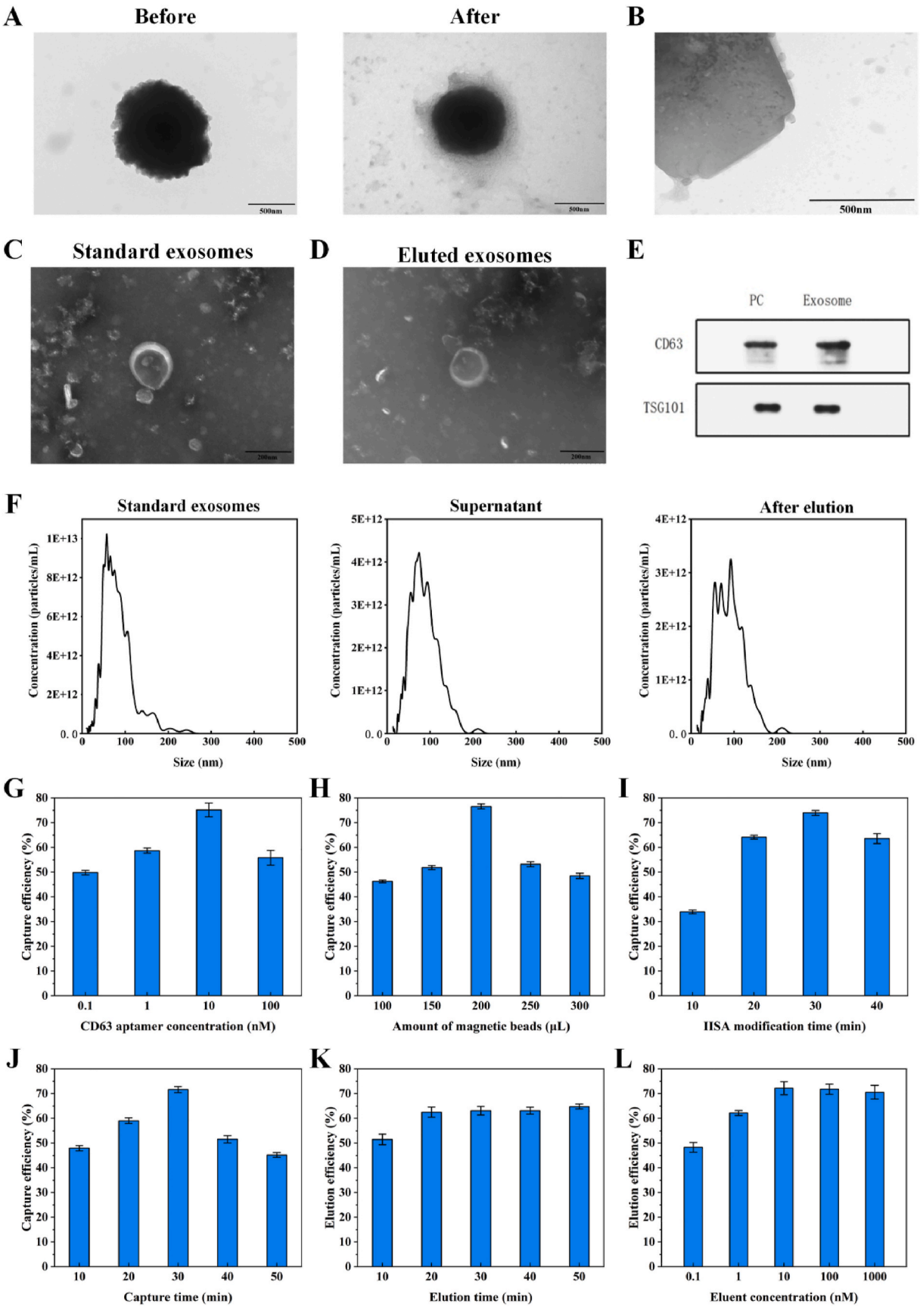
To optimize the system parameters, the ratio of Cas13a to crRNA was optimized using miRNA-21 as an example. The fluorescence profiles shown in Fig. 3I indicated that the fluorescence signals increased value with increasing ratio. However, by calculating the initial reaction rate (V0), we found that it peaked at 3:1 ratio and remained stable (Fig. 3J). The reaction rate was also affected by the reporter concentration. Fig. 3K illustrates the fluorescence curves of the CRISPR reaction at different reporter concentrations. The fluorescence inconsistently increased with reporter concentration and reached its peak value at 600 nM. By calculating V0 for each group (Fig. 3L), we found that V0 reached its maximum value when the reporter concentration was 600 nM. This is consistent with the results shown in Fig. 3K, in which excessively high concentrations does not result in a significant increase in the initial reaction rate.

To calculate the limits of detection (LOD) for the eight miRNAs, we performed linear regression analysis of V0 at different concentrations. The LODs (summarized in Fig. 3M) of the eight miRNAs were at the fM level, which is demonstrative of the high speed and high sensitivity of the assay. Fig. S5 shows that the relationship between the concentrations of the eight miRNAs and their V0s was linear within the dynamic detection range.

3.4. Characterization of the chip and on-chip exosome isolation and detection

At the microscale, the surface tension exerted onto the liquid can exceed gravity, forming a stable water/oil interface. This is an important factor in determining the experimental results. During the whole exosome isolation process on the chip, the water/oil interfaces need to be kept stable both at rest and during the dynamic gas-phase mixing process. To validate interface stability, we performed FLUENT simulations modeling water (Chamber 1) and oil (Chamber 2) as primary and secondary phases, respectively. Dynamic bubble mixing simulations revealed the interface stabilized at rounded corners within 40 s with clear demarcation (Fig. 4A). To visualize the test results, red ink was added to chambers 1, 3, and 5; and 10 % silicone oil solution was added to chambers 2 and 4 to observe interface movement. Fig. 4B illustrates the two-phase interface remained stable both at rest and during dynamic bubble mixing, with minimal movement. This indicates that bubble movement had a negligible effect on interfacial stability.

The structure of the chip to aid in mixing is a double-layer gas channel, modeled in FLUENT to assess the mixing performance of the two layers individually or combined. The Volume Fraction Difference



(caption on next page)

Fig. 2. Characterization of the results of exosome isolation using IISA. (A) TEM images of magnetic beads before and after Strep-tag II and CD63 aptamers modification. (B) TEM image of exosome after being captured by IISA. (C) TEM image of standard exosomes. (D) TEM image of eluted exosomes. (E) Western blot analysis of eluted exosomes. The band intensities for CD63 and TSG101 in PC (Standard exosomes) were 62 and 54, respectively. The band intensities for CD63 and TSG101 in eluted exosomes were 40 and 38, respectively. (F) Comparison of the size-concentration distribution curves of exosomes: in the supernatant after on-chip capture, in the elution, and with those of standard exosomes. (G) Variations of exosome capture efficiency of IISA with different aptamer concentrations. (H) Variations of exosome capture efficiency of IISA with different magnetic bead amounts. (I) Variations of exosome capture efficiency of IISA with different aptamer modification times. (J) Variations of exosome capture efficiency of IISA with different capture times. (K) Variations of exosome elution efficiency with different elution times. (L) Variations of exosome elution efficiency at different elution concentrations.

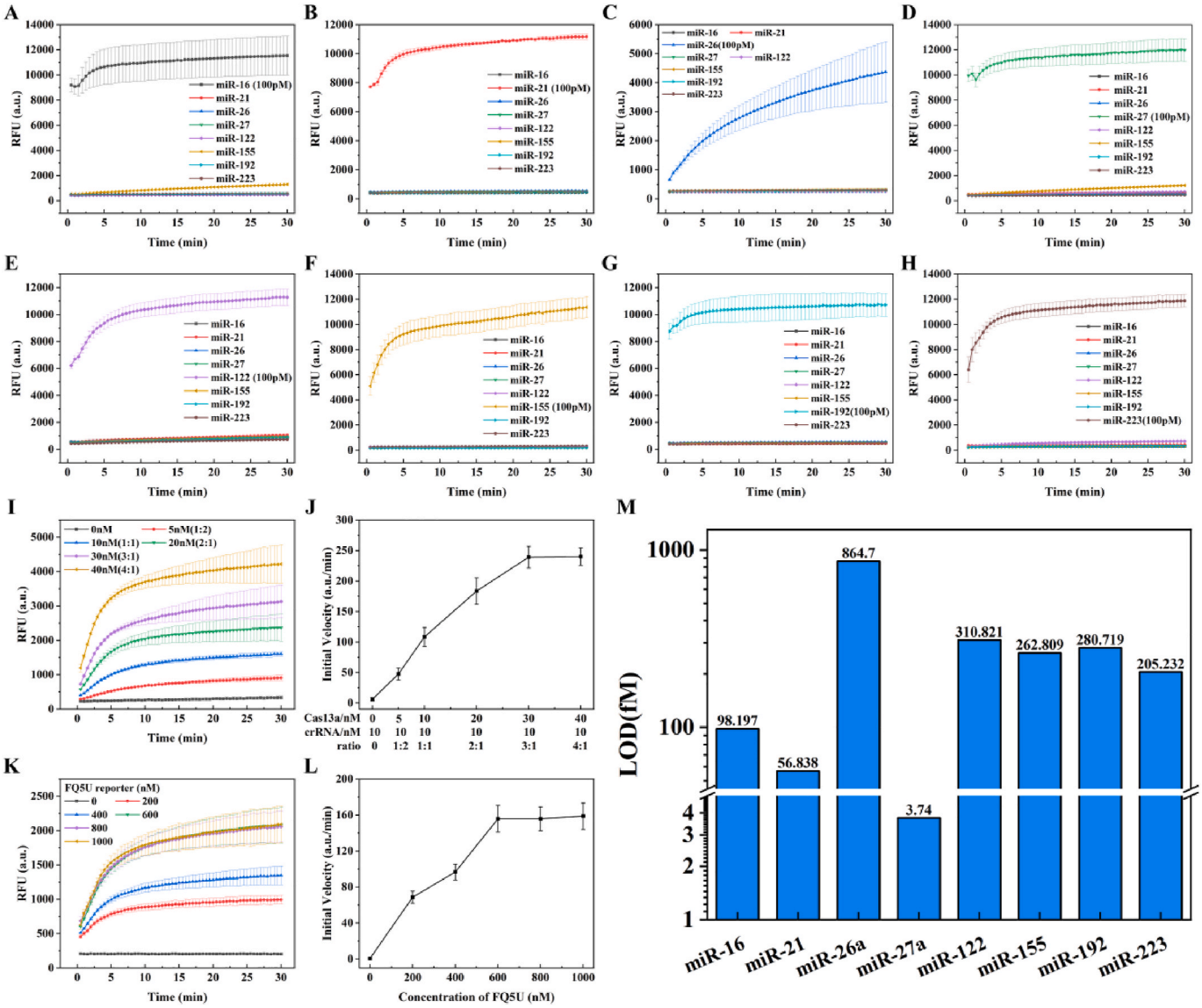


Fig. 3. Analysis of Cas13a/crRNA for miRNA detection. (A–H) Results from cross-over experiment of eight miRNAs. All experiments were conducted in a 10 μL system. The concentration of the target was 100 pM and the concentration of interfering miRNAs was 1 nM. The fluorescence signals of each reaction were obtained from the qPCR instrument at 30-s intervals. (I) Real-time fluorescence curves at different Cas13a/crRNA ratios (crRNA concentration was 10 nM and Cas13a concentrations were varied from 0 to 40 nM). (J) Calculated V0 at different Cas13a/crRNA ratios. (K) Real-time fluorescence curves at different reporter concentrations. (L) Calculated V0 at different reporter concentrations. (M) LOD of eight miRNAs. Each experiment was repeated three times.

(VFD) between two key planes was used as a quantitative metric, which includes PH1 at the initial partition interface and PH2 at the chamber's bottom surface. Fig. 4C shows VFD on the two planes of the three configurations over 5 s, indicating that the mixing performance with the double-layer setup was superior to others. The superior mixing effect of the double-layer channel was also evident in the cloud diagrams of aqueous phase distribution from simulations at the end of bubble mixing (Fig. S6A). To visualize the results, we added magnetic beads to the chip's chamber to observe and measure bubble mixing performance. The bead distribution before and after mixing (Fig. S6B) indicated effective bubble mixing at a gas injection rate of 0.02 m/s within 3 min, with optimal performance verified through flow rate calibration and additional simulations (Fig. S7).

The detection zone consists of eight cylindrical chambers connected to the recovery chamber via columnar channels. By calculating the pressures on both sides of the interface, we found that the pressure

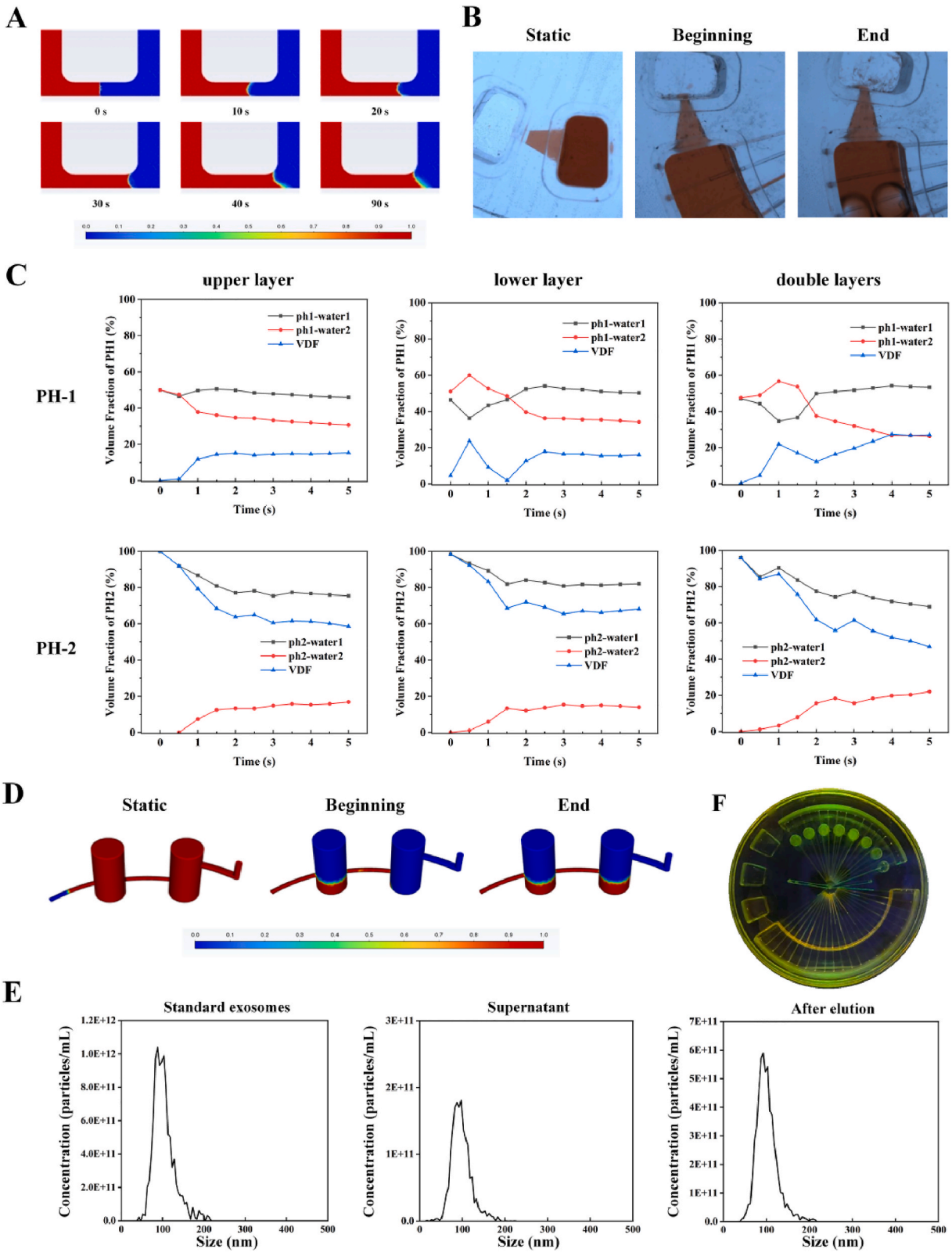


Fig. 4. Characterization of on-chip performance. (A) Simulation of the two-phase interface at different states. (C) Liquid volume fraction in two planes for single and double gas channel structures. (D) Simulation of liquid transfer through negative pressure. The three images show the distribution of the liquid at rest, at the beginning and at the end of the negative pressure drive. (E) Comparison of the size-concentration distribution curves of exosomes: in the supernatant after on-chip capture, in the elution, and with those of standard exosomes. (F) Fluorescent image of on-chip reactions (concentration of each of the eight miRNAs was 25 pM). The miRNAs detected in the eight chambers were (from left to right): miR-223, miR-155, miR-122, miR-192, miR-27, miR-16, miR-21, miR-26.

difference caused by the interfacial tension between the two phases exceeded that caused by the difference in liquid surface heights. Under static conditions, the interfacial tension prevented the spontaneous transfer of the liquid from the recovery chamber to the detection chamber. Therefore, an external negative pressure was applied to facilitate the simultaneous transfer of liquid into the eight chambers. FLUENT simulations (Fig. 4D) demonstrated complete liquid transfer within 12 s. Experimental validation using red ink in chamber 5 (Fig. S8) confirmed optimal transfer occurred at 12–14 s of negative pressure application, meeting detection requirements. The tops of the detection chambers were sealed, and an external pumping negative gas flow rate was set at 0.01 m/s.

We investigated the effect of the number of transfers on magnetic bead transfer efficiency and found that three repeated transfers essentially achieved the maximum transfer efficiency (Table S4). This protocol was used in subsequent experiments. Fig. 4E shows the size-concentration curves of exosomes measured by NTA after capture and elution, which matched the size criteria of standard exosomes. By statistically analyzing particle counts, we found that the capture efficiency for exosomes was ~78 % and the recovery rate was approximately 55 %, which is slightly lower than that of the off-chip experiments, possibly due to the reduced collection efficiency of the magnetic beads on the chip and the loss of some exosomes during the transfer process. Some magnetic beads capturing exosomes may have been lost when passing through the immiscible phase interface. Additionally, a small number of magnetic beads bound to exosomes may have been left in the dead spaces of the chip structure, leading to a reduction in the recovered exosomes.

To validate the CRISPR reactions on the chip, standard exosomes were lysed after being transferred to a recovery chamber, and a mixture of eight miRNAs was added. Then, the liquid was transferred by negative pressure into the eight detection chambers for reaction. Fig. 4F shows the fluorescence of the 10-min reactions on the chip, demonstrating the validity of on-chip CRISPR responses. To analyze the effect of exosomal lysis buffer on CRISPR reactions, we measured the fluorescence intensity of reactions containing different percentages of lysis buffer using miRNA-21 as an example. The results in Fig. S9 showed that exosomal lysis buffer had an inhibitory effect on the CRISPR reaction, which was minimized at a 30 % lysis buffer proportion in the reaction system.

3.5. Application in clinical samples

Based on previously optimized system parameters for exosome isolation and miRNA detection (as summarized in Table S6), we designed and fabricated an automated device (Fig. S10). The clinical samples consisted of serum samples from patients (experimental groups), and serum samples of healthy individuals (controls). The expression levels of different miRNAs can reflect pathological information for cancer diagnosis, treatment, and prognosis. The expression levels of various miRNAs in HCC tissues and the circulatory system are different (Hou et al., 2021; Matsuura et al., 2019; Wang et al. 2014, 2018, 2021).

To evaluate the expression levels of eight miRNAs in exosomes from the serum of HCC patients, we used the chip and qRT-PCR for analysis and comparison. The expression levels of eight miRNAs in samples from HCC patients were analyzed by qRT-PCR firstly, as depicted in Fig. 5A.

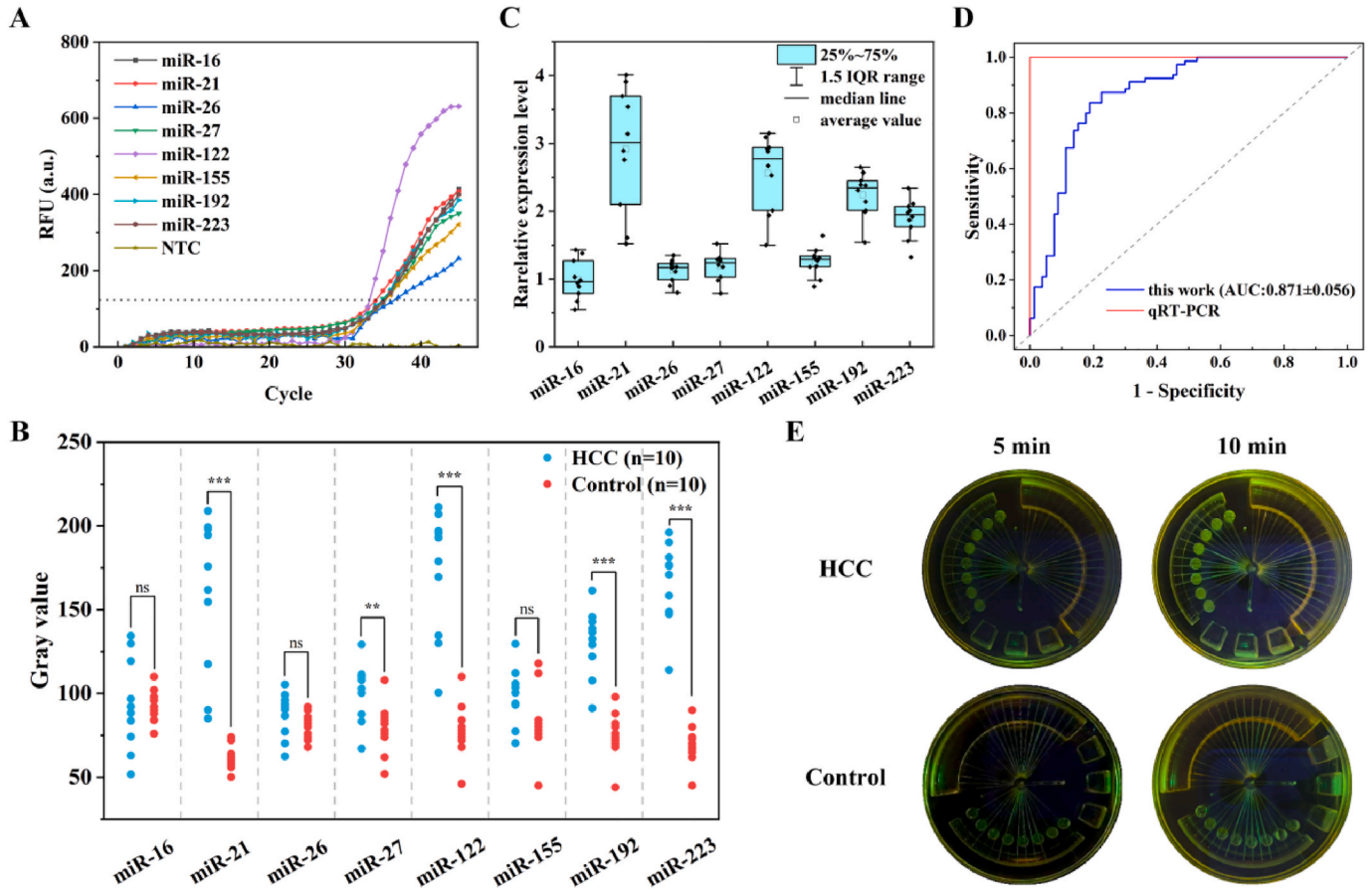


Fig. 5. Testing of clinical samples. (A) qRT-PCR results of serum samples from HCC patients. (B) Fluorescent gray values of serum samples from HCC patients and healthy individuals detected on-chip by CRISPR/Cas13a. (**p < 0.01, ***p < 0.001, "ns" for non-significant differences). (C) Expression levels of eight miRNAs in serum exosomes of HCC patients relative to healthy individuals ($control_{average} = 1$). (D) ROC plot of qRT-PCR and this chip in the detection of clinical samples. (E) Examples of fluorograms of serum samples from HCC patients and healthy individuals after reacting for 5–10 min on the chip.

Then, we demonstrated the varying expression levels of 20 samples by calculating the grayscale fluorescence values of on-chip CRISPR reactions in the detection chambers (Fig. 5B). The expression levels of the eight miRNAs differed between HCC patients and healthy individuals. Notably, miRNA-26, miRNA-155, and the internal reference miRNA-16 showed no significant difference in expression between the two groups. This may be attributed to several factors: (1) These miRNAs are known to have relatively low expression levels in both healthy and HCC tissues, which may make it more challenging to detect significant differences, especially with a limited sample size. (2) There is considerable individual variability in miRNA expression due to factors such as genetic background, lifestyle, and comorbidities. This variability may contribute to the lack of significant differences observed in our study. This highlights the importance of a combined multi-target detection, enabling more accurate assessment based on the overall results. Compared to the average expression levels of eight miRNAs in healthy population, we observed that the miRNA expression levels in serum exosomes of HCC patients were up-regulated to varying degrees (Fig. 5C). Comparing the specificity and sensitivity of qRT-PCR and this chip for the detection of clinical samples, Fig. 5D demonstrates the ROC plots of the two methods. Based on the calculations, the AUC value obtained from our chip was 0.871, indicating that the chip has significant potential for application in clinical samples detection. To demonstrate the on-chip reactions of clinical samples, the two groups of clinical samples were observed under a blue LED transilluminator (Fig. 5E). As can be seen, the fluorescence intensity of samples from HCC patients was notably higher than that of healthy population, and the intensity increased over time. These results demonstrate the feasibility of the chip in exosome isolation and miRNA detection and the quantification of exosomal miRNAs from serum samples. Exosomal miRNA detection better reflects HCC-specific molecular signatures while minimizing non-tumor background interference, significantly improving diagnostic accuracy.

4. Conclusion

Free miRNAs in circulation typically have short half-lives (minutes to hours) and are prone to degradation. In contrast, exosomal miRNAs better reflect HCC-related molecular signatures while reducing background noises from non-tumor sources. Therefore, HCC diagnostic accuracy can be enhanced by immunomagnetic exosome isolation before miRNA analysis and combined with multi-miRNAs detection. This study successfully achieved "sample-in, result-out" detection of multiple exosomal miRNAs within 1 h, marking the first study to realize the simultaneous detection of eight exosomal miRNAs. The chip captures exosomes using CD63 aptamers-modified magnetic beads, achieving high-purity isolation and enrichment within 35 min through integrated IFAST technology and gas-phase mixing. The downstream miRNA detection module simultaneously quantifies eight miRNAs, with multi-miRNA profiling providing complementary diagnostic insights to support accurate treatment decisions. The rapid and efficient detection of 20 samples demonstrates this chip's strong potential for clinical diagnostics. Compared with previous studies (Chinnappan et al., 2023; Jang et al., 2019; Peng et al., 2025), our system is more advantageous in terms of detection time, number of multiplexed tests, ease of use, and cost (comparisons are shown in Table S7 and costs are shown in Table S8). While the chip shows potential for cancer liquid biopsies and in-depth studies, further improvements in exosome recovery and miRNA detection sensitivity are needed. Significant progress has been made in recent years in the separation and detection of exosomes using electrochemical methods, which can realize the efficient separation and highly sensitive detection of exosomes (Ni et al., 2023; Yang et al., 2025). In the case of molecular detection of miRNAs and other molecules in exosomes, electrochemical-based technologies can achieve accurate detection and analysis with low background noise and high sensitivity (Li et al., 2016; Wang et al., 2022; Yang et al., 2023). In the future, we will focus on improving the sensitivity of exosomal miRNA detection to improve its clinical utility. Specifically, we aim to improve exosome separation efficiency by optimizing the immiscible interface, adjusting the magnet positions, and enhancing the magnetic field to minimize the loss of magnetic beads and exosomes or combining multiple isolation methods and enhance detection sensitivity through the introduction of digital single-molecule detection, cascade signal amplification techniques, electrochemical techniques or other signal enhancement techniques.

CRediT authorship contribution statement

Niancai Peng: Supervision, Project administration, Funding acquisition. **Xueqin Gao:** Writing – original draft, Validation, Methodology, Investigation. **Zhang Yong:** Writing – original draft, Methodology, Investigation, Conceptualization. **Yunyun Zhang:** Writing – review & editing, Methodology, Investigation. **Xiaoniu Guo:** Validation, Conceptualization. **Qiaochu Wang:** Validation, Investigation. **Yong Wan:** Supervision, Resources. **Shuhao Zhao:** Conceptualization. **Tianyi Zhang:** Supervision. **Fei Hu:** Writing – review & editing, Supervision, Funding acquisition, Conceptualization.

Funding

This research was funded by the National Natural Science Foundation of China (62375217), Key Research and Development Program of China (2021YFC2400902) and Shaanxi Province Key R&D Program (2020GXLH-Z-005).

Declaration of competing interest

The authors declare that they have no known competing financial interests or personal relationships that could have appeared to influence the work reported in this paper.

Acknowledgments

We thank all the members who made guidance and helped in the experiment.

Appendix A. Supplementary data

Supplementary data to this article can be found online at https://doi.org/10.1016/j.bios.2025.117460.

Data availability

Data will be made available on request.

References

Baranyai, T., Herczeg, K., Onódi, Z., Voszka, I., Módos, K., Marton, N., Nagy, G., Mäger, I., Wood, M.J., El Andaloussi, S., Pálinkás, Z., Kumar, V., Nagy, P., Kittel, A., Buzás, E.I., Ferdinandy, P., Giricz, Z., 2015. Isolation of exosomes from blood plasma: qualitative and quantitative comparison of ultracentrifugation and size exclusion chromatography methods. PLoS One 10 (12), e0145686. https://doi.org/10.1371/journal.pone.0145686.

Berry, S.M., Alarid, E.T., Beebe, D.J., 2011a. One-step purification of nucleic acid for gene expression analysis via Immiscible filtration assisted by surface tension (IFAST). Lab Chip 11 (10), 1747–1753. https://doi.org/10.1039/c1lc00004g.

Berry, S.M., LaVanway, A.J., Pezzi, H.M., Guckenberger, D.J., Anderson, M.A., Loeb, J. M., Beebe, D.J., 2014. HIV viral RNA extraction in wax immiscible filtration assisted by surface tension (IFAST) devices. J. Mol. Diagn. 16 (3), 297–304. https://doi.org/10.1016/j.jmoldx.2014.01.004.

Berry, S.M., Strotman, L.N., Kueck, J.D., Alarid, E.T., Beebe, D.J., 2011b. Purification of cell subpopulations via immiscible filtration assisted by surface tension (IFAST). Biomed. Microdevices 13 (6), 1033–1042. https://doi.org/10.1007/s10544-011-9573-z.

Bhattacharya, S., Steele, R., Shrivastava, S., Chakraborty, S., Di Bisceglie, A.M., Ray, R. B., 2016. Serum miR-30e and miR-223 as novel noninvasive biomarkers for hepatocellular carcinoma. Am. J. Pathol. 186 (2), 242–247. https://doi.org/10.1016/j.ajpath.2015.10.003.

Cao, Y.Q., Qin, Y.L., Cheng, Q.X., Zhong, J.L., Han, B., Li, Y., 2025. Bifunctional nanomaterial enabled high-specific isolation of urinary exosomes for cervical cancer metabolomics analysis and biomarker discovery. Talanta 285. https://doi.org/10.1016/j.talanta.2024.127280.

Chinnappan, R., Ramadan, Q., Zourob, M., 2023. An integrated lab-on-a-chip platform for pre-concentration and detection of colorectal cancer exosomes using anti-CD63 aptamer as a recognition element. Biosens. Bioelectron. 220, 114856. https://doi.org/10.1016/j.bios.2022.114856.

Fang, X.X., Chen, C., Liu, B., Ma, Z.J., Hu, F.L., Li, H.Y., Gu, H.C., Xu, H., 2021. A magnetic b ead-me diate d selective adsorption strategy for extracellular vesicle separation and purification. Acta Biomater. 124, 336–347. https://doi.org/10.1016/j.actbio.2021.02.004.

Fu, Y.J., Mackowiak, B., Feng, D.C., Lu, H.K., Guan, Y.K., Lehner, T., Pan, H.N., Wang, X. W., He, Y., Gao, B., 2023. MicroRNA-223 attenuates hepatocarcinogenesis by blocking hypoxia-driven angiogenesis and immunosuppression. Gut 72 (10), 1942–1958. https://doi.org/10.1136/gutjnl-2022-327924.

Gao, Y.K., Qiang, L., Chu, Y.J., Han, Y.K., Zhang, Y., Han, L., 2020. Microfluidic chip for multiple detection of miRNA biomarkers in breast cancer based on three-segment hybridization. AIP Adv. 10 (4), 045022. https://doi.org/10.1063/1.5137784.

Guo, X.N., Hu, F., Yong, Z., Zhao, S.H., Wan, Y., Wang, B.Q., Peng, N.C., 2024. Magnetic nanoparticle-based microfluidic platform for automated enrichment of high-purity extracellular vesicles. Anal. Chem. 96 (18), 7212–7219. https://doi.org/10.1021/acs.analchem.4c00795.

Guo, X.N., Hu, F., Zhao, S.H., Yong, Z., Zhang, Z.M., Peng, N.C., 2023. Immunomagnetic separation method integrated with the strep-tag II system for rapid enrichment and mild release of exosomes. Anal. Chem. 95 (7), 3569–3576. https://doi.org/10.1021/acs.analchem.2c03470.

Hou, X., Yin, S., Ren, R.X., Liu, S.Q., Yong, L., Liu, Y.X., Li, Y., Zheng, M.H., Kunos, G., Gao, B., Wang, H., 2021. Myeloid-cell-specific IL-6 signaling promotes MicroRNA-223-Enriched exosome production to attenuate NAFLD-associated fibrosis. Hepatology 74 (1), 116–132. https://doi.org/10.1002/hep.31658.

Jablonska, J., Pietrowska, M., Ludwig, S., Lang, S., Thakur, B.K., 2019. Challenges in the isolation and proteomic analysis of cancer exosomes-implications for translational research. Proteomes 7 (2), 22. https://doi.org/10.3390/proteomes7020022.

Jang, M., Choi, G., Choi, Y.Y., Lee, J.E., Jung, J.H., Oh, S.W., Han, D.H., Lee, H., Park, J. H., Cheong, J.H., Kim, P., 2019. Extracellular vesicle (EV)-Polyphenol nanoaggregates for microRNA-based cancer diagnosis. NPG Asia Mater. 11, 79. https://doi.org/10.1038/s41427-019-0184-0.

Kaarj, K., Akarapipad, P., Yoon, J.Y., 2018. Simpler, faster, and sensitive zika virus assay using smartphone detection of loop-mediated isothermal amplification on paper microfluidic chips. Sci. Rep. 8 (1), 12438. https://doi.org/10.1038/s41598-018-30797-9.

Kalluri, R., LeBleu, V.S., 2020. The biology, function, and biomedical applications of exosomes. Science 367 (6478), eaau6977. https://doi.org/10.1126/science.aau6977.

Keerthikumar, S., Chisanga, D., Ariyaratne, D., Saffar, H., Anand, S., Zhao, K.N., Samuel, M., Pathan, M., Jois, M., Chilamkurti, N., Gangoda, L., Mathivanan, S., 2016. ExoCarta: a web-based compendium of exosomal cargo. J. Mol. Biol. 428 (4), 688–692. https://doi.org/10.1016/j.jmb.2015.09.019.

Lee, S.H., Brianna, 2024. Association of microRNA-21 expression with breast cancer subtypes and its potential as an early biomarker. Pathol. Res. Pract. 254, 155073. https://doi.org/10.1016/j.prp.2023.155073.

Li, C., Wu, D., Hu, X.L., Xiang, Y., Shu, Y.Q., Li, G.X., 2016. One-step modification of electrode surface for ultrasensitive and highly selective detection of nucleic acids with practical applications. Anal. Chem. 88 (15), 7583–7590. https://doi.org/10.1021/acs.analchem.6b01250.

Liu, X.L., Pan, Q., Cao, H.X., Xin, F.Z., Zhao, Z.H., Yang, R.X., Zeng, J., Zhou, H.P., Fan, J. G., 2020. Lipotoxic hepatocyte-derived exosomal MicroRNA 192-5p activates macrophages through rictor/Akt/Forkhead box transcription factor O1 signaling in nonalcoholic fatty liver disease. Hepatology 72 (2), 454–469. https://doi.org/10.1002/hep.31050.

Matsuura, Y., Wada, H., Eguchi, H., Gotoh, K., Kobayashi, S., Kinoshita, M., Kubo, M., Hayashi, K., Iwagami, Y., Yamada, D., Asaoka, T., Noda, T., Kawamoto, K., Takeda, Y., Tanemura, M., Umeshita, K., Doki, Y., Mori, M., 2019. Exosomal miR-155 derived from hepatocellular carcinoma cells under hypoxia promotes angiogenesis in endothelial cells. Dig. Dis. Sci. 64 (3), 792–802. https://doi.org/10.1007/s10620-018-5380-1.

Ngamsom, B., Truyts, A., Fourie, L., Kumar, S., Tarn, M.D., Iles, A., Moodley, K., Land, K. J., Pamme, N., 2017. A microfluidic device for rapid screening of E-coli O157:H7 based on IFAST and ATP bioluminescence assay for water analysis. Chem. Eur J. 23 (52), 12754–12757. https://doi.org/10.1002/chem.201703487.

Ni, M., Wu, X.Y., Gui, Y.Y., Huang, Y., Wang, F., Li, C., 2023. A dual metal-organic framework-based electrochemical biosensor for the capture and detection of cancerous exosomes. ACS Appl. Nano Mater. 6 (19), 18614–18622. https://doi.org/10.1021/acsanm.3c04336.

O'Brien, K., Breyne, K., Ughetto, S., Laurent, L.C., Breakefield, X.O., 2020. RNA delivery by extracellular vesicles in Mammalian cells and its applications. Nat. Rev. Mol. Cell Biol. 21 (10), 585–606. https://doi.org/10.1038/s41580-020-0251-y.

Öksüz, Z., Gragnani, L., Lorini, S., Temel, G.O., Serin, M.S., Zignego, A.L., 2023. Evaluation of plasma miR-17-5p, miR-24-3p and miRNA-223-3p profile of hepatitis C virus-infected patients after treatment with direct-acting antivirals. J. Pers. Med. 13 (8), 1188. https://doi.org/10.3390/jpm13081188.

Peng, J., Li, B.C., Ma, Z.Y., Qiu, Z.X., Hu, H., Jiang, Y.Y., Gao, D., 2025. A microfluidic-based chemiluminescence biosensor for sensitive multiplex detection of exosomal microRNAs based on hybridization chain reaction. Talanta 281. https://doi.org/10.1016/j.talanta.2024.126838.

Pritchard, C.C., Cheng, H.H., Tewari, M., 2012. MicroRNA profiling: approaches and considerations. Nat. Rev. Genet. 13 (5), 358–369. https://doi.org/10.1038/nrg3198.

Qian, Q., Wei, Y., Xu, Y., Zheng, M., Wang, C., Zhang, S., Xie, X., Ye, C., Mi, X., 2023. Microfluidic magnetic detection system combined with a DNA framework-mediated immune-sandwich assay for rapid and sensitive detection of tumor-derived exosomes. Microsyst. Nanoeng. 9 (6), 139. https://doi.org/10.1038/s41378-023-00617-w.

Qin, P.W., Park, M., Alfson, K.J., Tamhankar, M., Carrion, R., Patterson, J.L., Griffiths, A., He, Q., Yildiz, A., Mathies, R., Du, K., 2019. Rapid and fully microfluidic ebola virus detection with CRISPR-Cas13a. ACS Sens. 4 (4), 1048–1054. https://doi.org/10.1021/acssensors.9b00239.

Sasaki, R., Kanda, T., Yokosuka, O., Kato, N., Matsuoka, S., Moriyama, M., 2019. Exosomes and hepatocellular carcinoma: from bench to bedside. Int. J. Mol. Sci. 20 (6), 1406. https://doi.org/10.3390/ijms20061406.

Shan, Y., Zhou, X., Huang, R., Xing, D., 2019. High-fidelity and rapid quantification of miRNA combining crRNA programmability and CRISPR/Cas13a trans-Cleavage activity. Anal. Chem. 91 (8), 5278–5285. https://doi.org/10.1021/acs.analchem.9b00073.

Sidhom, K., Obi, P.O., Saleem, A., 2020. A review of exosomal isolation methods: is size exclusion chromatography the best option? Int. J. Mol. Sci. 21 (18), 6466. https://doi.org/10.3390/ijms21186466.

Ulep, T.H., Zenhausern, R., Gonzales, A., Knoff, D.S., Diaz, P.A.L., Castro, J.E., Yoon, J.Y., 2020. Smartphone based on-chip fluorescence imaging and capillary flow velocity measurement for detecting ROR1+cancer cells from buffy coat blood samples on dual-layer paper microfluidic chip. Biosens. Bioelectron. 153, 112042. https://doi.org/10.1016/j.bios.2020.112042.

Wang, F., Gui, Y.Y., Liu, W.T., Li, C., Yang, Y.C., 2022. Precise molecular profiling of circulating exosomes using a metal-organic framework-based sensing interface and an enzyme-based electrochemical logic platform. Anal. Chem. 94 (2), 875–883. https://doi.org/10.1021/acs.analchem.1c03644.

Wang, H., Hou, L., Li, A., Duan, Y., Gao, H., Song, X., 2014. Expression of serum exosomal microRNA-21 in human hepatocellular carcinoma. BioMed Res. Int. 2014, 864894. https://doi.org/10.1155/2014/864894.

Wang, N.Y., Wang, Q., Shen, D., Sun, X., Cao, X.M., Wu, D., 2016. Downregulation of microRNA-122 promotes proliferation, migration, and invasion of human hepatocellular carcinoma cells by activating epithelial-mesenchymal transition. OncoTargets Ther. 9, 2035–2047. https://doi.org/10.2147/ott.S92378.

Wang, R.X., Zhao, X.X., Chen, X.H., Qiu, X.P., Qing, G.C., Zhang, H., Zhang, L.L., Hu, X. L., He, Z.Q., Zhong, D.D., Wang, Y., Luo, Y., 2020. Rolling circular amplification (RCA)-assisted CRISPR/Cas9 cleavage (RACE) for highly specific detection of multiple extracellular vesicle MicroRNAs. Anal. Chem. 92 (2), 2176–2185. https://doi.org/10.1021/acs.analchem.9b04814.

Wang, X., He, Y., Mackowiak, B., Gao, B., 2021. MicroRNAs as regulators, biomarkers and therapeutic targets in liver diseases. Gut 70 (4), 784–795. https://doi.org/10.1136/gutjnl-2020-322526.

Wang, Y.R., Zhang, C.Y., Zhang, P.J., Guo, G.H., Jiang, T., Zhao, X.M., Jiang, J.J., Huang, X.L., Tong, H.L., Tian, Y.P., 2018. Serum exosomal microRNAs combined with alpha-fetoprotein as diagnostic markers of hepatocellular carcinoma. Cancer Med. 7 (5), 1670–1679. https://doi.org/10.1002/cam4.1390. -US.

Weber, J.A., Baxter, D.H., Zhang, S.L., Huang, D.Y., Huang, K.H., Lee, M.J., Galas, D.J., Wang, K., 2010. The MicroRNA spectrum in 12 body fluids. Clin. Chem. 56 (11), 1733–1741. https://doi.org/10.1373/clinchem.2010.147405.

Woo, H.K., Sunkara, V., Park, J., Kim, T.H., Han, J.R., Kim, C.J., Choi, H.I., Kim, Y.K., Cho, Y.K., 2017. Exodisc for rapid, size-selective, and efficient isolation and analysis of nanoscale extracellular vesicles from biological samples. ACS Nano 11 (2), 1360–1370. https://doi.org/10.1021/acsnano.6b06131.

Wu, H., Chen, X.Y., Zhang, M.Y., Wang, X.F., Chen, Y.J., Qian, C., Wu, J., Xu, J.F., 2021. Versatile detection with CRISPR/cas system from applications to challenges. TrAC Trends Anal. Chem. 135, 116150. https://doi.org/10.1016/j.trac.2020.116150.

Xu, G., Gao, Y., Yan, M., 2018. Expression of miR-155/PTEN axis in hepatocellular carcinoma and its mechanism. Cancer Res. Prev. Treat. 45 (2), 67–72. https://doi.org/10.3971/j.issn.1000-8578.2018.17.0931.

Xu, J.A., Wu, C., Che, X., Wang, L., Yu, D.K., Zhang, T.W., Huang, L.M., Li, H., Tan, W., Wang, C.F., Lin, D.X., 2011. Circulating MicroRNAs, miR-21, miR-122, and miR-223, in patients with hepatocellular carcinoma or chronic hepatitis. Mol. Carcinog. 50 (2), 136–142. https://doi.org/10.1002/mc.20712.

Yang, L.M., Guo, H., Gao, Q., Hou, T., Zhang, J.A., Liu, X.J., Li, F., 2023. Integrating reliable Pt-S bond-mediated 3D DNA nanomachine with magnetic separation in a homogeneous electrochemical strategy for exosomal MicroRNA detection with low background and high sensitivity. Anal. Chem. 95 (48), 17834–17842. https://doi.org/10.1021/acs.analchem.3c03914.

Yang, L.M., Zhang, J.G., Zhang, J., Hou, T., Gao, Q., Liu, X.J., Li, F., 2025. CRISPR-based homogeneous electrochemical strategy for near-zero background detection of breast cancer extracellular vesicles via fluidity-enhanced magnetic capture nanoprobe. Anal. Chem. 97 (4), 2176–2185. https://doi.org/10.1021/acs.analchem.4c05181.

Yang, X., Zhang, X.F., Lu, X., Jia, H.L., Liang, L., Dong, Q.Z., Ye, Q.H., Qin, L.X., 2014. MicroRNA-26a suppresses angiogenesis in human hepatocellular carcinoma by targeting hepatocyte growth Factor-cMet pathway. Hepatology 59 (5), 1874–1885. https://doi.org/10.1002/hep.26941.

Yang, Y.X., Yang, J.Z., Gong, F., Zuo, P.F., Tan, Z.Y., Li, J.J., Xie, C.H., Ji, X.H., Li, W.H., He, Z.K., 2022. Combining CRISPR/Cas12a with isothermal exponential amplification as an ultrasensitive sensing platform for microRNA detection. Sensor. Actuat. B-Chem. 367, 132158. https://doi.org/10.1016/j.snb.2022.132158.

Yu, J.J., Wei, Y., Cui, Z.P., Tian, J., Cai, H.B., Zhang, W.A., 2024. Thermosensitive capturer coupled with the CD63 aptamer for highly efficient isolation of exosomes. ACS Macro Lett. 13 (2), 195–200. https://doi.org/10.1021/acsmacrolett.3c00682.

Yu, W., Hurley, J., Roberts, D., Chakrabortty, S.K., Enderle, D., Noerholm, M., Breakefield, X.O., Skog, J.K., 2021a. Exosome-based liquid biopsies in cancer: opportunities and challenges. Ann. Oncol. 32 (4), 466–477. https://doi.org/10.1016/j.annonc.2021.01.074.

Yu, Z.X., Lin, S.J., Xia, F.F., Liu, Y.L., Zhang, D., Wang, F., Wang, Y.P., Li, Q.C., Niu, J.Q., Cao, C.X., Cui, D.X., Sheng, N.Q., Ren, J.Z., Wang, Z.G., Chen, D., 2021b. ExoSD chips for high-purity immunomagnetic separation and high-sensitivity detection of gastric cancer cell-derived exosomes. Biosens. Bioelectron. 194, 113594. https://doi.org/10.1016/j.bios.2021.113594.

Yuan, C.Q., Tian, T., Sun, J., Hu, M.L., Wang, X.S., Xiong, E.H., Cheng, M., Bao, Y.J., Lin, W., Jiang, J.M., Yang, C.W., Chen, Q., Zhang, H., Wang, H., Wang, X.R., Deng, X. B., Liao, X.P., Liu, Y.H., Wang, Z., Zhang, G.H., Zhou, X.M., 2020. Universal and naked-eye gene detection platform based on the clustered regularly interspaced short palindromic Repeats/Cas12a/13a system. Anal. Chem. 92 (5), 4029–4037. https://doi.org/10.1021/acs.analchem.9b05597.

Zhang, J.C., Cao, Z., Yang, G., You, L., Zhang, T.P., Zhao, Y.P., 2019a. MicroRNA-27a (miR-27a) in solid tumors: a review based on mechanisms and clinical observations. Front. Oncol. 9, 893. https://doi.org/10.3389/fonc.2019.00893.

Zhang, J.L., Huang, Y.H., Sun, M., Wan, S., Yang, C.Y., Song, Y.L., 2022. Recent advances in aptamer-based liquid biopsy. ACS Appl. Bio Mater. 5 (5), 1954–1979. https://doi.org/10.1021/acsabm.1c01202.

Zhang, K.X., Yue, Y.L., Wu, S.X., Liu, W., Shi, J.J., Zhang, Z.Z., 2019b. Rapid capture and nondestructive release of extracellular vesicles using aptamer-based magnetic isolation. ACS Sens. 4 (5), 1245–1251. https://doi.org/10.1021/acssensors.9b00060.

Zhao, J.H., Zhu, W.J., Mao, Y.X., Li, X.D., Ling, G.X., Luo, C., Zhang, P., 2024. Unignored intracellular journey and biomedical applications of extracellular vesicles. Adv. Drug Deliv. Rev. 212, 115388. https://doi.org/10.1016/j.addr.2024.115388.

Zhao, X.X., Zhang, W.Q., Qiu, X.P., Mei, Q., Luo, Y., Fu, W.L., 2020. Rapid and sensitive exosome detection with CRISPR/Cas12a. Anal. Bioanal. Chem. 412 (3), 601–609. https://doi.org/10.1007/s00216-019-02211-4.

Zhou, T., Huang, R., Huang, M.Q., Shen, J.J., Shan, Y.Y., Xing, D., 2020. CRISPR/Cas13a powered portable electrochemiluminescence chip for ultrasensitive and specific MiRNA detection. Adv. Sci. 7 (13), 1903661. https://doi.org/10.1002/advs.201903661.